Article

ENDOR Characterization of a Synthetic Diiron Hydrazido Complex as a Model for Nitrogenase Intermediates

Nicholas S. Lees, Rebecca L. McNaughton, Wilda Vargas Gregory, Patrick L. Holland, and Brian M. Hoffman

J. Am. Chem. Soc., **2008**, 130 (2), 546-555 • DOI: 10.1021/ja073934x

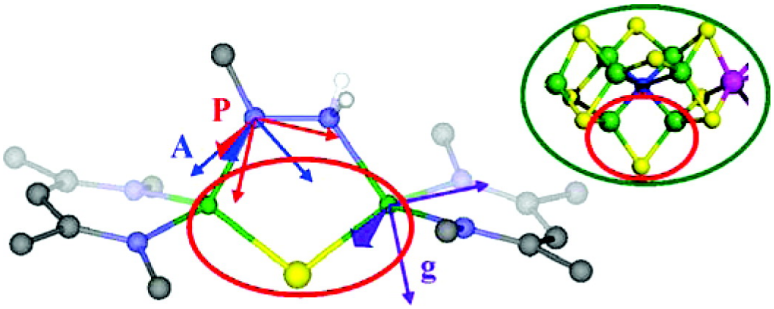

J|A|C|S
ARTICLES
Published on Web 12/20/2007

ENDOR Characterization of a Synthetic Diiron Hydrazido Complex as a Model for Nitrogenase Intermediates

Nicholas S. Lees,[†] Rebecca L. McNaughton,[†] Wilda Vargas Gregory,[‡] Patrick L. Holland,*[,‡] and Brian M. Hoffman*[,†]

Department of Chemistry, Northwestern University, 2145 Sheridan Road, Evanston, Illinois 60208 and Department of Chemistry, University of Rochester, RC Box 270216, Rochester, New York 14627-0216

Received June 7, 2007; E-mail: bmh@northwestern.edu

Abstract: Molybdenum-dependent nitrogenase binds and reduces N_2 at the [Fe_7, Mo, S_9, X, homocitrate] iron-molybdenum cofactor (FeMo-co). Kinetic and spectroscopic studies of nitrogenase variants indicate that a single Fe−S face is the most likely binding site. Recently, substantial progress has been made in determining the structures of nitrogenase intermediates formed during alkyne and N_2 reduction through use of ENDOR spectroscopy. However, constraints derived from ENDOR studies of biomimetic complexes with known structure would powerfully contribute in turning experimentally derived ENDOR parameters into structures for species bound to FeMo-co during N_2 reduction. The first report of a paramagnetic Fe−S compound that binds reduced forms of N_2 involved Fe complexes stabilized by a bulky β-diketiminate ligand (Vela, J.; Stoian, S.; Flaschenriem, C. J.; Münck, E.; Holland, P. L. *J. Am. Chem. Soc.* **2004**, *126*, 4522−4523). Treatment of a sulfidodiiron(II) complex with phenylhydrazine gave an isolable mixed-valence Fe^{II}−Fe^{III} complex with a bridging phenylhydrazido ($PhNNH_2$) ligand, and this species now has been characterized by ENDOR spectroscopy. Using both ^{15}N, ^{2}H labeled and unlabeled forms of the hydrazido ligand, the hyperfine and quadrupole parameters of the -N−NH_2 moiety have been derived by a procedure that incorporates the (near-) mirror symmetry of the complex and involves a strategy which combines experiment with semiempirical and DFT computations. The results support the use of DFT computations in identifying nitrogenous species bound to FeMo-co of nitrogenase turnover intermediates and indicate that ^{14}N quadrupole parameters from nitrogenase intermediates will provide a strong indication of the nature of the bound nitrogenous species. Comparison of the large ^{14}N hyperfine couplings measured here with that of a hydrazine-derived species bound to FeMo-co of a trapped nitrogenase intermediate suggests that the ion(s) are not high spin and/or that the spin coupling coefficients of the coordinating cofactor iron ion(s) in the intermediate are exceptionally small.

Introduction

Biological nitrogen fixation is catalyzed by the metalloenzyme nitrogenase according to the stoichiometry:[2,3]

$$N_2 + 8e^- + 8H^+ + 16MgATP \rightarrow 2NH_3 + H_2 + 16MgADP + 16\ Pi$$

Of the three types of nitrogenases,[4] the best studied and most prevalent is the Mo-dependent enzyme.[3] It is comprised of two catalytic components: the Fe protein contains a [4Fe-4S] cluster and delivers electrons to the MoFe protein, which contains the beautiful and complex [Fe_7, Mo, S_9, X, homocitrate] FeMo-cofactor active site, Figure 1.[5−8] It is widely assumed that N_2 reduction by nitrogenase involves a series of FeMo-co-bound nitrogenous species[2,3,9,10] beginning with bound N_2 and proceeding through the 2-electron/2-proton, semireduced intermediates of Scheme 1. However, this is by no means certain,[11,12] and

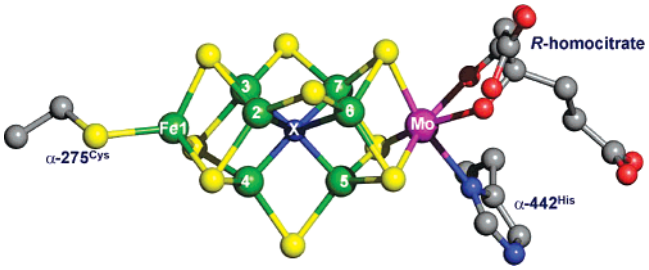

Figure 1. Structure of FeMo-cofactor, [Fe_7, Mo, S_9, X, homocitrate]; Fe2−7 are called the "waist" irons; X = N, C, or O.[5−8]

[†] Northwestern University.
[‡] University of Rochester.

(1) Vela, J.; Stoian, S.; Flaschenriem, C. J.; Münck, E.; Holland, P. L. *J. Am. Chem. Soc.* **2004**, *126*, 4522−4523.
(2) Christiansen, J.; Dean, D. R.; Seefeldt, L. C. *Annu. Rev. Plant Physiol. Plant Mol. Biol.* **2001**, *52*, 269−295.
(3) Burgess, B. K.; Lowe, D. L. *Chem. Rev.* **1996**, *96*, 2983−3011.
(4) Eady, R. R. *Chem. Rev.* **1996**, *96*, 3013−3030.
(5) Kim, J.; Rees, D. C. *Science* **1992**, *257*, 1677−1682.
(6) Kim, J.; Rees, D. C. *Nature* **1992**, *360*, 553−560.
(7) Chan, M. K.; Kim, J.; Rees, D. C. *Science* **1993**, *260*, 792−794.
(8) Einsle, O.; Tezcan, F. A.; Andrade, S. L. A.; Schmid, B.; Yoshida, M.; Howard, J. B.; Rees, D. C. *Science* **2002**, *297*, 1696−1700.
(9) Chatt, J.; Dilworth, J. R.; Richards, R. L. *Chem. Rev.* **1978**, *78*, 589−625.
(10) Thorneley, R. N. F.; Eady, R. R.; Lowe, D. J. *Nature* **1978**, *272*, 557−558.
(11) Schrock, R. R. *Acc. Chem. Res.* **2005**, *38*, 955−962.
(12) Schrock, R. R. *Proc. Natl. Acad. Sci. U.S.A.* **2006**, *103*, 17087.

10.1021/ja073934x CCC: $40.75

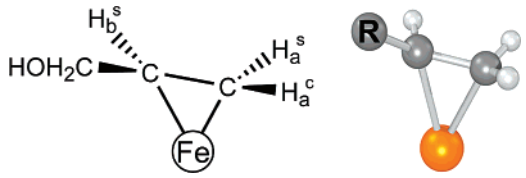

Figure 2. ENDOR-determined structure of the FeMo-co-bound allyl alcohol product of propargyl alcohol reduction by nitrogenase.[18]

Scheme 1

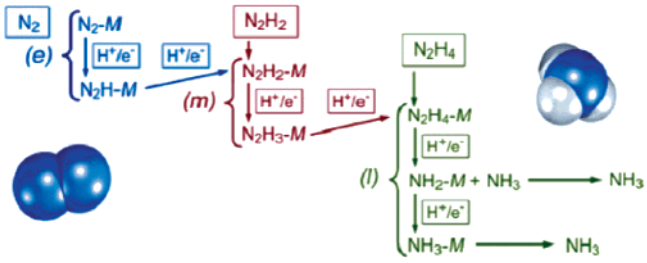

recently it has been shown that this assumption has important mechanistic implications.[13]

The major barrier to characterizing the nitrogenase catalytic mechanism has been the impossibility of synchronizing the delivery of electrons so that intermediates along the N_2 reduction pathway can be accumulated in high occupancy for characterization.[14] Recently, however, there has been remarkable progress in accumulating enzymatic intermediates for study. Enzymatic intermediates were first trapped by freeze quenching during the inhibition of turnover by CO,[15] during the reduction of alkyne substrates,[16−18] and during the reduction of H^+ under Ar.[19] ENDOR[20,21] and ESEEM[22] spectroscopies proved to be the methods of choice for characterizing substrate-derived species bound to FeMo-co in freeze-trapped nitrogenase intermediates. The first determination of the structure of such a species involved an intermediate formed during the reduction of propargyl alcohol (PA).[23] Analysis of the $^{1,2}H$ and ^{13}C ENDOR signals for the intermediate in the context of constraints provided by the structures of relevant inorganic model compounds led to the discovery that the intermediate contains the product of PA reduction, allyl alcohol, and is directly bound to FeMo-co in the ferracycle organometallic structure of Figure 2.[18] This assignment was subsequently supported by experiment[24] and DFT computations;[25] the latter further identified the particular Fe ion binding site. A corresponding species was trapped during reduction of C_2H_2 to C_2H_4 by nitrogenase α-195^{Gln} MoFe.[26]

Chart 1

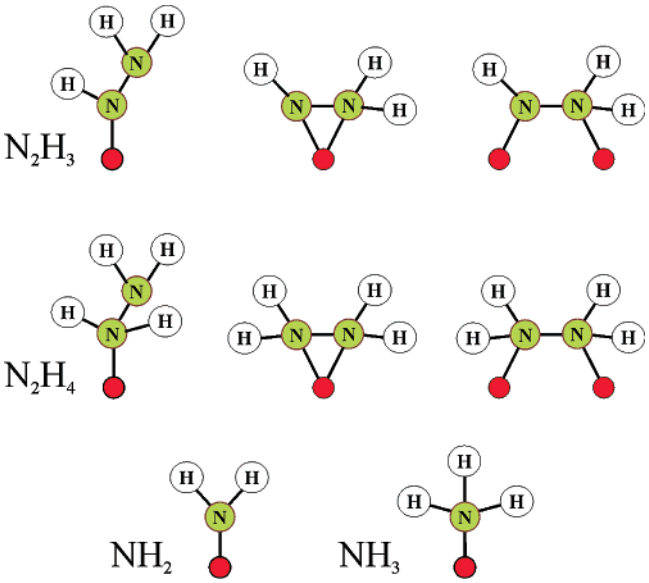

During the reduction of H^+ under Ar, an intermediate was trapped that has two hydrides bound to FeMo-co[19] and is the state activated for N_2 binding by the accumulation of four e^-/H^+.[27]

No EPR signals from any intermediate of N_2 reduction had been detected until a series of publications[13,28−31] described species trapped during reduction of N_2, $CH_3N{=}NH$, N_2H_2, and N_2H_4. We posited that the state formed during reduction of N_2 by WT MoFe represents an early catalytic nitrogenase intermediate (Scheme 1), denoted $e(N_2)$, whereas those trapped during turnover with the other substrates have converged to a single late intermediate, denoted $l(N_2H_4)$, with a nitrogenous species that is at least at the reduction level of N_2H_4 bound to FeMo-co.

The task of determining the structures of FeMo-co-bound species derived from the natural substrate, N_2, is substantially more challenging than the determination that an η^2-alkene structure forms during alkyne reduction. The latter reaction stops with the alkene as final product, leaving the C−C bond intact, whereas N_2 reduction ultimately cleaves the N−N bond so it is not even known *a priori* whether an intermediate contains a FeMo-co-bound species with one or two N atoms. Further, the C−H bonds of an alkene do not exchange in water and it is possible to use selective deuteration to assist in quantitating the number of C−H, whereas all the N−H of a nitrogenous intermediate are exchangeable and it is not. The multiplicity of species that must be considered for any N_2-reduction intermediate is illustrated by sketches of some of the possible structures for nitrogenous species bound to Fe atoms of the FeMoco "waist" in later stages of the catalytic process, Chart 1.

(13) Barney, B. M.; Lukoyanov, D.; Yang, T.-C.; Dean, D. R.; Hoffman, B. M.; Seefeldt, L. C. *Proc. Natl. Acad. Sci. U.S.A.* **2006**, *103*, 17113−17118.
(14) Seefeldt, L. C.; Dance, I. G.; Dean, D. R. *Biochemistry* **2004**, *43*, 1401−1409.
(15) Lee, H.-I.; Cameron, L. M.; Hales, B. J.; Hoffman, B. M. *J. Am. Chem. Soc.* **1997**, *119*, 10121−10126.
(16) Lee, H.-I.; Sorlie, M.; Christiansen, J.; Song, R.; Dean, D. R.; Hales, B. J.; Hoffman, B. M. *J. Am. Chem. Soc.* **2000**, *122*, 5582−5587.
(17) Dos Santos, P. C.; Igarashi, R. Y.; Lee, H.-I.; Hoffman, B. M.; Seefeldt, L. C.; Dean, D. R. *Acc. Chem. Res.* **2005**, *38*, 208−214.
(18) Lee, H.-I.; Igarashi, R. Y.; Laryukhin, M.; Doan, P. E.; Dos, Santos, P. C.; Dean, D. R.; Seefeldt, L. C.; Hoffman, B. M. *J. Am. Chem. Soc.* **2004**, *126*, 9563−9569.
(19) Igarashi, R. Y.; Laryukhin, M.; Santos, P. C. D.; Lee, H.-I.; Dean, D. R.; Seefeldt, L. C.; Hoffman, B. M. *J. Am. Chem. Soc.* **2005**, *127*, 6231−6241.
(20) Hoffman, B. M. *Acc. Chem. Res.* **2003**, *36*, 522−529.
(21) Hoffman, B. *Proc. Natl. Acad. Sci. U.S.A.* **2003**, *100*, 3575−3578.
(22) Deligiannakis, Y.; Louloudi, M.; Hadjiliadis, N. *Coord. Chem. Rev.* **2000**, *204*, 1−112.
(23) Benton, P. M. C.; Laryukhin, M.; Mayer, S. M.; Hoffman, B. M.; Dean, D. R.; Seefeldt, L. C. *Biochemistry* **2003**, *42*, 9102−9109.
(24) Igarashi, R. Y.; Dos Santos, P. C.; Niehaus, W. G.; Dance, I. G.; Dean, D. R.; Seefeldt, L. C. *J. Biol. Chem.* **2004**, *279*, 34770−34775.
(25) Dance, I. *J. Am. Chem. Soc.* **2004**, *126*, 11852−11863.
(26) Lee, H.-I.; Sørlie, M.; Christiansen, J.; Yang, T.-C.; Shao, J.; Dean, D. R.; Hales, B. J.; Hoffman, B. M. *J. Am. Chem. Soc.* **2005**, *127*, 15880−15890.
(27) Lukoyanov, D.; Barney, B. M.; Dean, D. R.; Seefeldt, L. C.; Hoffman, B. M. *Proc. Natl. Acad. Sci. U.S.A.* **2007**, *104*, 1451−1455.
(28) Barney, B. M.; Igarashi, R. Y.; Dos, Santos, P. C.; Dean, D. R.; Seefeldt, L. C. *J. Biol. Chem.* **2004**, *279*, 53621−53624.
(29) Barney, B. M.; Laryukhin, M.; Igarashi, R. Y.; Lee, H.-I.; Santos, P. C. D.; Yang, T.-C.; Hoffman, B. M.; Dean, D. R.; Seefeldt, L. C. *Biochemistry* **2005**, *44*, 8030−8037.
(30) Barney, B. M.; Yang, T.-C.; Igarashi, R. Y.; Santos, P. C. D.; Laryukhin, M.; Lee, H.-I.; Hoffman, B. M.; Dean, D. R.; Seefeldt, L. C. *J. Am. Chem. Soc.* **2005**, *127*, 14960−14961.
(31) Seefeldt, L. C.; Dean, D. R.; Hoffman, B. M.; Dos Santos, P. C.; Barney, B. M.; Lee, H.-I. *Dalton Trans.* **2006**, 2277−2284.

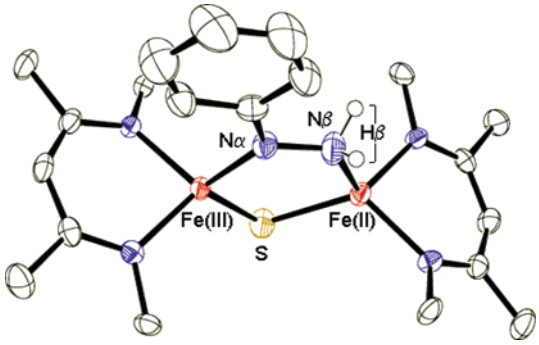

Figure 3. Crystal structure of **1**, as reported by Vela et al.[1] 50% ellipsoids, C-bound H atoms, and aryl groups omitted.

One of the aims of ENDOR spectroscopic studies of N_2-reduction intermediates[13,28−31] is to determine the number and equivalence/inequivalence (if there are two) of the N atoms, as well as the number and distribution of N-bound H atoms, that comprise the nitrogenous species bound to FeMo-co. As can be seen in Chart 1, such information would eliminate many of the possible assignments for a nitrogenase intermediate. This effort would be greatly aided by comparing the hyperfine coupling parameters of the bound species with those of well-defined biomimetic complexes that have structures like those in Chart 1. However, until recently, no appropriate complexes were available. The first report of a paramagnetic Fe−S compound that binds reduced forms of N_2 involved Fe complexes stabilized by a bulky β-diketiminate ligand.[1,32] Treatment of a sulfidodiiron(II) complex with phenylhydrazine gave an excellent analog of a four-electron/three-proton reduced form of N_2 bound to the "waist" of the nitrogenase FeMo-co: an isolable mixed-valence $Fe^{II}-Fe^{III}$ complex (**1**) with a bridging phenylhydrazido ($PhNNH_2$) ligand, Figure 3.[1] Mössbauer and EPR studies showed that the complex contains high-spin Fe ions coupled antiferromagnetically to give an $S = {}^1/_2$ ground state. Interestingly, **1** contains both formally anionic N-donor and neutral N-donor atoms, providing an opportunity to define coupling parameters for both types of Fe−N bond simultaneously.

In this report, we present a detailed ENDOR study of **1**, the first for any model of a possible nitrogenase intermediate. $Ph^{15}NH^{15}NH_2$ and $PhN^2HN^2H_2$ were used to synthesize **1**(^{15}N) and **1**(^{2}H) respectively. The electron−nuclear (hyperfine) and nuclear (quadrupole) coupling parameters of the nitrogen and hydrogen atoms of the bound hydrazide of **1** have been obtained through a novel procedure that both incorporates the (near-) mirror symmetry of **1** and employs a strategy for combining ENDOR experiment and analysis with semiempirical and DFT computations. We use the measured parameters to calibrate DFT computations of such intermediates and discuss how the coupling parameters can be used as constraints to test proposed structures of reduced forms of N_2 bound to FeMo-co in nitrogenase intermediates.

Materials and Methods

Synthesis. ^{15}N-Labeled Phenylhydrazine. $Ph^{15}NH_2$ was diazotized with $Na^{15}NO_2$ and reduced with $SnCl_2$ using a literature method,[33] giving $Ph^{15}NH^{15}NH_2$·HCl. This compound was deprotonated with NaOH, extracted into benzene, dried over 4 Å molecular sieves, and crystallized from dry diethyl ether at −40 °C in the drybox. The ^{1}H NMR resonances at $\delta = 4.40$ and 2.67 ppm were doublets with ^{15}N−^{1}H coupling constants of 89 and 69 Hz, respectively.

^{2}H-Labeled Phenylhydrazine. $PhN^2HN^2H_2$ was synthesized by refluxing a mixture of $PhNHNH_2$ (Aldrich, 5 mL), D_2O (10 mL), and conc. HCl (5 drops) overnight under N_2. After removal of volatile materials, it was transferred to the drybox, extracted with dry diethyl ether, filtered, and cooled to −40 °C to give crystalline product. Full deuteration was confirmed using ^{1}H NMR and ^{2}H NMR spectroscopy.

Sample Preparation. The mixed-valence hydrazidodiiron complexes were prepared as previously described,[1] using phenylhydrazine or its isotopomers. Spectroscopic samples (60 μL of a 1.8 mM solution in toluene) were prepared in the drybox and placed in a 2 mm I.D. quartz tube. After stopping the open end of the tube with a plug of silicone grease, the tube was brought out of the drybox and cooled to 77 K for shipment and storage.

Spectroscopy. Spectrometers used for 35 GHz CW EPR[34] and Pulsed ENDOR[35] spectroscopies, described earlier, are equipped with helium immersion dewars for measurements at ~2 K. ENDOR measurements employed either the Mims[36] or reMims[37] pulse sequence for small hyperfine couplings or the Davies pulse sequence[36] for large couplings. For further details, see Supporting Information.

DFT Calculations. Version 2005.01 of the Amsterdam Density Functional (ADF)[38−40] package was used for all computations with a spin-unrestricted formalism and the BLYP exchange functional consisting of the Becke exchange gradient[41] and Lee−Yang−Parr correlation[42] corrections. The complete crystal structure geometry of **1** was directly imported as the molecular coordinates. The TZP basis set, as implemented in ADF as triple-ζ Slater-type orbitals, was used for all atoms. No frozen core potentials were used, and the integral accuracy was set to 6.0. Computations on a pared-down input molecule, where all the phenyl groups except that of the hydrazine were replaced by H, were tested with the larger TZ2P basis set but no significant differences resulted. Complex **1** contains two magnetic metal centers that are antiferromagnetically spin-coupled, and we used the broken symmetry (BS) method developed by Noodleman and co-workers to model the antiferromagnetic state.[43,44] A single-point calculation of **1** in the high-spin state ($S = {}^9/_2$) formed from a high-spin Fe(III) ($S = {}^5/_2$) that binds Nα and high-spin Fe(II) ($S = 2$) that binds Nβ was computed first. The resulting α and β electron densities on the Fe(II) were permutated to generate the initial potential for the BS spin-flipped ($S = {}^1/_2$) calculation. Hyperfine and quadrupole tensors were calculated for each state with the standard ESR[45] and QTENS[46] keywords as implemented in ADF. Previous applications of the BS method have shown that the *electron* density of the spin-flipped state corresponds to the electron density of the true antiferromagnetic state and the nuclear quadrupole coupling tensors resulting from this calculation can be directly compared to experimental results.[47,48] However, this is not the case for the *spin* density, so the computed hyperfine tensors of the bridging atoms of interest must be corrected by spin-projection. The specific spin-projection method employed in this paper is given in Supporting Information and further detail will be given elsewhere.[49]

(32) Holland, P. L. *Can. J. Chem.* **2005**, *83*, 296−301.
(33) Conn, R. S. E.; Douglas, A. W.; Karady, S.; Corley, E. G.; Lovell, A. V.; Shinkai, I. *J. Org. Chem.* **1990**, *55*, 2908−2913.
(34) Werst, M. M.; Davoust, C. E.; Hoffman, B. M. *J. Am. Chem. Soc.* **1991**, *113*, 1533−1538.
(35) Davoust, C. E.; Doan, P. E.; Hoffman, B. M. *J. Magn. Reson.* **1996**, *119*, 38−44.
(36) Schweiger, A.; Jeschke, G. *Principles of Pulse Electron Paramagnetic Resonance*; Oxford University Press: Oxford, UK, 2001.
(37) Doan, P. E.; Hoffman, B. M. *Chem. Phys. Lett.* **1997**, *269*, 208−214.
(38) Te Velde, G.; Bickelhaupt, F. M.; Baerends, E. J.; Fonseca Guerra, C.; Van Gisbergen, S. J. A.; Snijders, J. G.; Ziegler, T. *J. Compu. Chem.* **2001**, *22*, 931−967.
(39) Guerra, C. F.; Snijders, J. G.; Te Velde, G.; Baerends, E. J. *Theor. Chem. Acc.* **1998**, *99*, 391−403.
(40) ADF2005.01, SCM, Theoretical Chemistry, Vrije Universiteit, Amsterdam, The Netherlands, http://www.scm.com.
(41) Becke, A. D. *Phys. Rev. A: At., Mol., Opt. Phys.* **1988**, *38*, 3098−3100.
(42) Lee, C.; Yang, W.; Parr, R. G. *Phys. Rev. B: Condens. Matter Mater. Phys.* **1988**, *37*, 785−789.
(43) Noodleman, L. *J. Chem. Phys.* **1981**, *74*, 5737−5743.
(44) Mouesca, J.-M.; Chen, J. L.; Noodleman, L.; Bashford, D.; Case, D. A. *J. Am. Chem. Soc.* **1994**, *116*, 11898−11914.

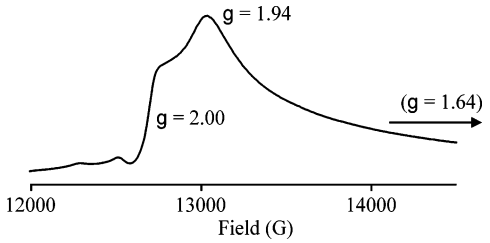

Figure 4. Absorption-display CW EPR spectrum of **1**. Low-intensity peaks below low-field edge of primary spectrum are due to minor impurities of unknown composition, which make no contribution to the ENDOR data. MW frequency = 35.316 GHz.

Results

EPR. The 35 GHz CW EPR spectrum of **1** has a rhombic **g** tensor, **g** = [2.00, 1.94, 1.64], Figure 4,[50] characteristic of a mixed-valence diiron center in which a high-spin Fe(III), $S = {}^5/_2$, is strongly antiferromagnetically coupled to a high-spin Fe(II), $S = 2$, to yield a ground state of total spin $S = {}^1/_2$.[1,32] The crystal structure of **1** of course does not reveal the oxidation state of the two iron atoms, but simple considerations of charge require that Fe(III) binds the negatively charged, deprotonated "central" Nα of the phenylhydrazide ligand, Fe(II) the terminal Nβ (Figure 3). The orientation of **g** in the molecular coordinate frame is determined below through analysis of ENDOR measurements.

ENDOR. Davies 35 GHz pulsed ENDOR spectra of **1** reveal numerous ^{14}N peaks in the 3−25 MHz range and ^{1}H peaks in the 40−70 MHz region. To identify the signals from the Fe-bound $PhNNH_2$ moiety and to fully characterize them required ENDOR data from the natural-abundance sample and from samples that incorporated $Ph^{15}N^{15}NH_2$, **1**(^{15}N), and $PhNN^2H_2$, **1**(^{2}H).

Full characterization of a $PhNNH_2$ nucleus hyperfine-coupled to the diiron center requires determination of its hyperfine tensor, **A**, as well as the determination of the quadrupole tensor, **P**, for a ^{14}N ($I = 1$). This involves analysis of a 2D field-frequency pattern comprised of ENDOR spectra collected at numerous fields across the EPR envelope of the center.[20,21,51−53] The analysis yields the principal values of **A**, **P**, and their orientations relative to the **g** tensor coordinate frame. The final step is to determine the orientations of **g**, **A**, and **P** relative to the molecular frame. This task is simplified by the mirror symmetry of the molecule in the FeNNFeS plane. As the exchange-coupled Fe ions lie in this plane, **g** must show mirror symmetry: one g value must lie normal to that plane, whereas the other g-orientations lie in the mirror plane. This means that the orientation of **g** is fixed by determining which g direction lies normal to the plane plus the angle, θ, between one in-plane direction and the Fe−Fe vector. Likewise, the two N lie in the plane and the **A**($^{14/15}$N), **P**(^{14}N) tensors must show the mirror symmetry of **g**, with one principal direction of **A**($^{14/15}$N), **P**(^{14}N) lying along the g value normal to the plane.

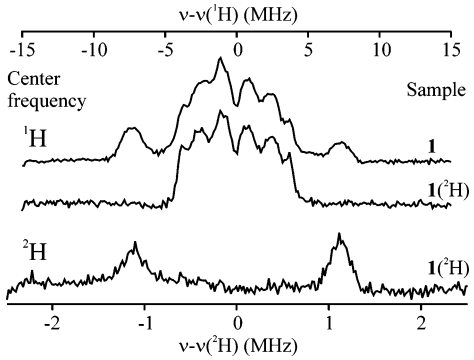

Figure 5. Pulsed ^{1}H ENDOR spectra of **1** and **1**(^{2}H); ^{2}H spectrum of **1**(^{2}H). The ^{1}H and ^{2}H frequency axes have been scaled according to the ratio of the nuclear g values of ^{1}H and ^{2}H. Spectra collected at g = 1.74: ^{1}H spectra: Davies pulse sequence, π pulse length = 80 ns, τ = 700 ns, repetition time = 5 ms, MW frequency = 34.987 GHz (**1**), 35.049 GHz (**1**(^{2}H)); ^{2}H spectrum: reMims pulse sequence, $\pi/2$ pulse length = 32 ns, τ = 200 ns, repetition time = 5 ms, MW frequency = 35.030 GHz.

The 2D^{1,2}H ENDOR patterns also are determined by the molecular symmetry, but in a more complex way. The two Hβ are chemically equivalent and the two N-^{2}H bonds are related by reflection through the molecular mirror plane that bisects the Hβ−N−Hβ angle. Thus, the two Hβ also are *magnetically* equivalent and must have identical 2D ENDOR patterns, so the observed pattern will exhibit a single *type* of ^{1,2}Hβ.

The analysis of the ^{14,15}N ENDOR data, given below, identifies the g-value that lies along the normal to the molecular mirror plane as g_1. Incorporation of this result into the analysis of the^{1,2}H ENDOR data fixes the orientation of [g_2, g_3] within the molecular plane; this orientation is specified by the angle θ between g_3 and the Fe−Fe vector. It is most convenient to begin the presentation by describing a ^{1,2}H ENDOR analysis that assumes that g_1 is normal to the mirror and then justifying this assumption in the subsequent description of the ^{14,15}N ENDOR analysis.

^{1,2}H ENDOR. Figure 5 presents 35 GHz Davies pulsed ^{1}H ENDOR spectra of **1**(^{1,2}H) and refocused Mims pulsed ^{2}H ENDOR spectra of **1**(^{2}H), all collected at g = 1.74 (close to g_3). The ^{1}H pulsed-ENDOR exhibits a doublet split by A(^{1}H) = 13 MHz plus at least three doublets with splittings of less than 10 MHz. The strongly coupled ^{1}H doublet is shown to be from Hβ by its loss upon deuterium exchange of the two Hβ protons; in parallel, the ^{2}H spectrum of the deuterated sample, **1**(^{2}H), reveals a single ^{2}Hβ doublet that has the same hyperfine coupling when scaled by the nuclear g factors, Figure 5. The observation of only one doublet due to both Hβ at g_3 (and all other g values, see below) is expected from the symmetry considerations discussed above.

2D field-frequency patterns were generated by collecting 35 GHz Davies pulsed ^{1}H ENDOR spectra of **1**(^{1,2}H) and re-Mims pulsed ^{2}H ENDOR spectra of **1**(^{2}H) at numerous fields across the entire EPR envelope, Figure 6. Over much of the EPR envelope, the ^{1}Hβ signals overlap the signals from the more weakly coupled, nonexchangeable protons, whereas there are no other ^{2}H signals to interfere with those from ^{2}Hβ. We henceforth discuss only the ^{2}Hβ ENDOR results, dropping the isotope label when a remark is valid for both ^{1,2}H.

The strong variation of the ^{2}Hβ doublet splitting across the 2D pattern, Figure 6, shows that the Hβ coupling is significantly

(45) van Lenthe, E.; van der Avoird, A.; Wormer, P. E. S. *J. Chem. Phys.* **1998**, *108*, 4783−4796.
(46) van Lenthe, E.; Jan Baerends, E. *J. Chem. Phys.* **2000**, *112*, 8279−8292.
(47) Han, W.-G.; Lovell, T.; Liu, T.; Noodleman, L. *Inorg. Chem.* **2003**, *42*, 2751−2758.
(48) Sinnecker, S.; Neese, F.; Noodleman, L.; Lubitz, W. *J. Am. Chem. Soc.* **2004**, *126*, 2613−2622.
(49) McNaughton, R. L.; Hoffman, B. M. Manuscript in preparation.
(50) All samples exhibited weak signals at higher g values (Figure 4) from impurities of unknown composition. ENDOR signals were not obtainable from these species, and thus, their presence is ignored.
(51) Hoffman, B. M.; DeRose, V. J.; Doan, P. E.; Gurbiel, R. J.; Houseman, A. L. P.; Telser, J. *Biol. Magn. Reson.* **1993**, *13(EMR of Paramagnetic Molecules)*, 151−218.
(52) DeRose, V. J.; Hoffman, B. M. In *Methods Enzymology*; Sauer, K., Ed.; Academic Press: New York, 1995; Vol. 246, pp 554−589.
(53) Doan, P. E. In *Paramagnetic Resonance of Metallobiomolecules*; Telser, J., Ed.; American Chemical Society: Washington, D.C., 2003; pp 55−81.

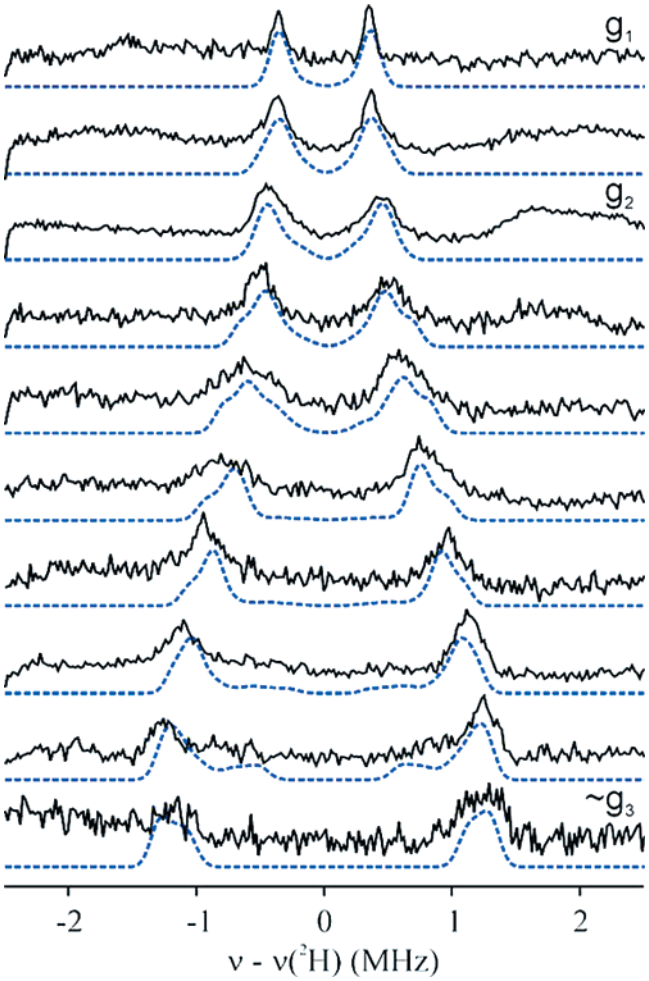

Figure 6. Simulated (blue) and experimental (black) 2D Field-frequency plot of reMims ^{2}H ENDOR spectra for **1**(^{2}H), normalized to unity for convenience. Conditions: $\pi/2$ pulse length = 32 ns, τ = 200 ns, repetition time = 5 ms, average MW frequency = 35.05 GHz. Simulation parameters (determined as described in text): **g** = [2.00, 1.94, 1.64], **A** = [−1.0, 0.7, 2.8] MHz (Euler angles $\alpha = 20$, $\beta = 15$, $\gamma = 50$), line width = 0.15 MHz. An essential feature of these simulations is their incorporation of the Mims ENDOR response function, R (eq S3), as discussed in Supporting Information.

anisotropic. The hyperfine tensor describing this pattern was arrived at through an iterative procedure in which calculations of the anisotropic hyperfine interaction were used to guide analysis of the 2D ENDOR pattern. Our earlier work with mixed-valence diiron centers[54,55] shows that the hyperfine tensor for Hβ (**A**(H)) of **1** will be dominated by the through-space electron−nuclear dipolar interaction with the spin-coupled diiron core (**T**(H)), with the possible addition of a small isotropic coupling: **A**(H) = **T**(H) + a_{iso}. This work further indicates that **T**(H) will be quite accurately reproduced by a point-dipole calculation of the anisotropic interaction tensor for the Hβ protons, $\mathbf{T}^{\mathbf{Dip}}$(H) (Table 1), through use of equations presented earlier.[54,55] To assist the ENDOR analysis of both the ^{1,2}H and ^{14,15}N hyperfine and quadrupole tensors of the coordinated hydrazine, broken-symmetry DFT calculations were performed on the crystal structure of **1**; for analysis of the ^{1,2}H ENDOR, the principal values of the DFT hyperfine tensor for Hβ ($\mathbf{A}^{\mathbf{DFT}}$-(^{2}H), Table 1) was decomposed into isotropic and anisotropic components, $a_{iso}^{DFT}(^2H)$, $\mathbf{T}^{\mathbf{DFT}}(^2H)$.

The two calculated Hβ dipole tensors are in excellent agreement and are almost completely rhombic, namely **T** ≈ [T, 0, −T]: $\mathbf{T}^{\mathbf{Dip}}(^2H)$ = [T_1, T_2, T_3] = [−2.4, 0.4, 2.0] MHz; $\mathbf{T}^{\mathbf{DFT}}$-(^{2}H) = [−2.6, 0.4, 2.2] MHz. The orientations of $\mathbf{T}^{\mathbf{Dip}}(^2H)$ and $\mathbf{T}^{\mathbf{DFT}}(^2H)$ also are in good agreement. The large positive T_3 and negative T_1 lie in the FeFeHβ plane which is tilted approximately 14° from the molecular mirror plane; this plane is shaded in Figure 7. This is exactly true by definition for $\mathbf{T}^{\mathbf{Dip}}$-(^{2}H), and is very close for $\mathbf{T}^{\mathbf{DFT}}(^2H)$. Table 1 contains the direction cosines of the principal directions in the molecular frame, as defined in Figure 7, with *Z* along the Fe−Fe direction, and *X* perpendicular to the FeNNFeS mirror plane. The orientation of $\mathbf{T}^{\mathbf{Dip}}(^2H)$ is also shown in the figure.

$\mathbf{T}^{\mathbf{Dip}}(^2H)$ was used as the starting point for a determination of the experimental hyperfine tensor **T**(^{2}H) through simulation of the 2D ^{2}H ENDOR pattern of Figure 6.[56] In the process, we completed the determination of the orientation of **g** relative to the molecular frame. A simulation of the 2D ^{2}H ENDOR pattern yields the orientation of **T**(^{2}H) relative to the **g** frame; the calculation of $\mathbf{T}^{\mathbf{Dip}}(^2H)$ specifies its orientation relative to the molecular frame. The three-stage procedure described in Appendix I (see Supporting Information) yields a best-fit **A**(^{2}H) whose orientation relative to the molecular frame is known through its relation to the orientation of $\mathbf{T}^{\mathbf{Dip}}(^2H)$; then the orientation of **g** relative to **T**(^{2}H), as derived from the simulations, (transitively) specifies the orientation of **g** in the molecular frame.

The optimized experimental **A**(^{2}H) principal values, along with the direction cosines of the principal directions relative to the molecular frame, are given in Table 1; Figure 7 shows the corresponding orientation of **A**(^{2}H) relative to the molecular frame, along with the orientation of $\mathbf{A}^{\mathbf{Dip}}(^2H)$, calculated with the dipolar model. As expected, the experimental orientation of **A** is almost indistinguishable from that of $\mathbf{T}^{\mathbf{dip}}$; the differences will be discussed below.

Considering the orientation of **g**, as discussed above g_1 is normal to the molecular mirror plane and thus the orientation of **g** relative to the molecular plane is completely defined by specifying θ, the angle between g_3 and the Fe−Fe vector (Figure 7). The analysis procedure of Appendix I yields a best-fit value, $\theta = 12$; the optimized orientation of **g** is shown in Figure 11, below.

$^{14/15}$N ENDOR. Figure 8 compares Davies pulsed ENDOR spectra collected at g_1 from **1** and **1**(^{15}N) prepared with doubly ^{15}N labeled hydrazine. The spectrum of **1** shows numerous features that are associated with the ^{14}N of the β-diketiminate ligand and that do not change upon labeling the hydrazide. In addition, a pair of peaks at 12 and 18 MHz is lost in the **1**(^{15}N) spectrum and thus must be associated with a hydrazide ^{14}N ($I = 1$). Accompanying this loss there appears a single peak at 21 MHz in **1**(^{15}N) that must be associated with a ^{15}N ($I = {}^1/_2$) of the hydrazide. As shown in the figure, the two ^{14}N peaks from hydrazide of **1**(^{14}N) can be assigned as the quadrupole-split ν doublet from a single ^{14}N atom with A(^{14}N) = 22 MHz and quadrupole splitting, $3P(g_1) = 6$ MHz, whereas the ^{15}N peak corresponds to the ν_+ feature of a doublet with |A(^{15}N)| = 31 MHz value predicted when the Larmor and hyperfine frequen-

(54) Willems, J.-P.; Lee, H.-I.; Burdi, D.; Doan, P. E.; Stubbe, J.; Hoffman, B. M. *J. Am. Chem. Soc.* **1997**, *119*, 9816−9824.
(55) DeRose, V. J.; Liu, K. E.; Lippard, S. J.; Hoffman, B. M. *J. Am. Chem. Soc.* **1996**, *118*, 121−134.

(56) For completeness, we note the 2D pattern of Figure 6 also can be described by a hyperfine tensor dominated not by the dipolar interaction but by the isotropic coupling, even though such a description disagrees with both the point-dipole and DFT calculations. However, this alternative is ruled out by an extended Mims ENDOR investigation (Supporting Information).

Table 1. Calculated and Experimental Hyperfine Tensors (MHz) of $^2H\beta$

	dipolar calculation			DFT calculation			simulation		
A		−		−1.7	1.3	3.1	−1.0	0.7	2.8
a_{iso}		−		0.9			0.8		
T	−2.4	0.4	2.0	−2.6	0.4	2.2	−1.8	−0.1	1.9
M(A_{mol}) (Tensor axis direction cosines)	−0.21	0.97	−0.11	−0.22	0.97	−0.04	−0.32	0.93	−0.17
	0.87	0.24	0.43	0.89	0.22	0.39	0.84	0.36	0.40
	0.44	0	−0.90	0.39	0.05	−0.92	0.43	−0.01	−0.90
θ(deg)	104	14	104	104	13	96	111	21	113
ϕ(deg)	64	90	154	67	87	157	65	91	155

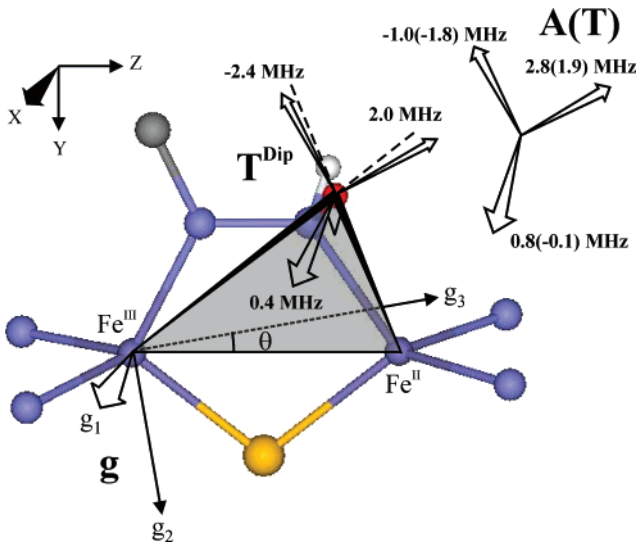

Figure 7. Model used in calculating and simulating ^2H ENDOR spectra of **1**(^2H). The **g** tensor lies in the FeNNFeS plane, with g_2 and g_3 at an orientation within the plane defined by θ, as shown. The **T** tensor for the "red" ^2H lies in the Fe^{2}H plane (shaded region), with the dipolar components shown exactly as calculated, as described in the text. The experimentally determined **A** (and **T**) tensor is shown at the top right.

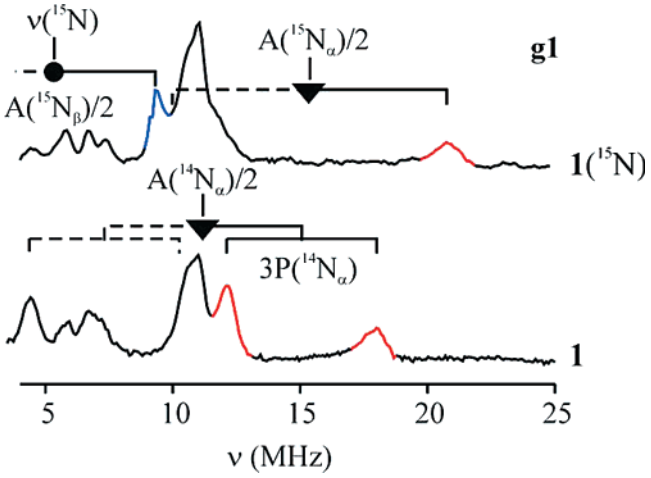

Figure 8. Davies ENDOR spectra collected at g_1 from **1** and **1**(^{15}N) showing ^{14}N peaks for **1**, both ^{15}N peaks from the labeled hydrazide ligand and ^{14}N from the β−diketiminate ligand for **1**(^{15}N). Peaks shown in red are assigned to hydrazide Nα, peaks shown in blue to hydrazide Nβ. Conditions: π pulse length = 80 ns, τ = 700 ns, repetition time = 5 ms, MW frequency **1**(^{15}N) = 35.037 GHz, **1** = 35.069 GHz.

cies are scaled by the ratio of the nuclear g values. The ν_- partner for the ^{15}N peak is not resolved, due to overlap with other nitrogen peaks, and may be undetectable regardless. A peak at 4.5 MHz in the **1**(^{14}N) spectrum most likely corresponds to one of the ν_- quadrupole split partners for the ^{14}N peak.

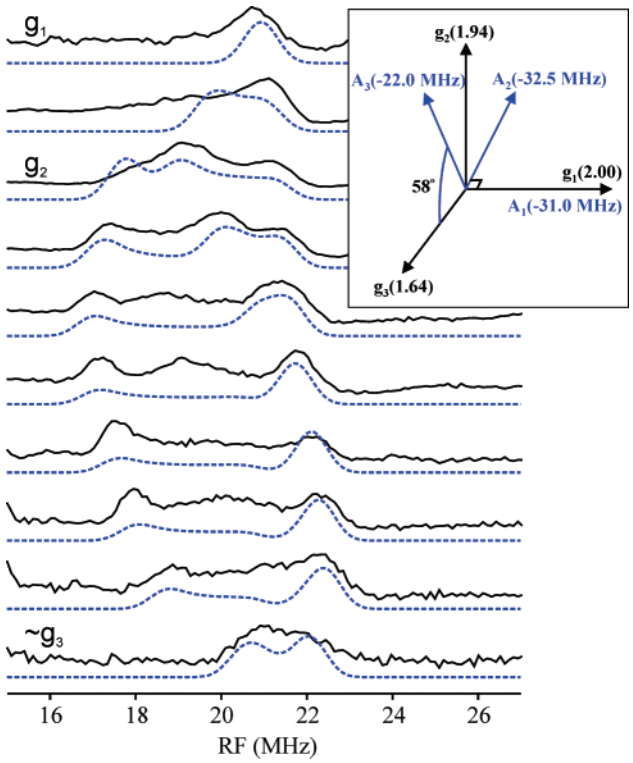

Figure 9. Simulated (blue) and experimental (black) 2D Field-frequency plot of ^{15}N Davies ENDOR spectra for **1**(^{15}N), normalized to unity as in Figure 6. Conditions: π pulse length = 80 ns, τ = 700 ns, repetition time = 5 ms, MW frequency = 35.037 GHz. We note that it is commonly the case that the relative ENDOR intensity predicted by a simulation will not perfectly match the experiment in some areas, as here in the spectrum between g_1 and g_2. This arises from EPR and ENDOR line width, transition probability, and spin-diffusion phenomena that are not included in simulations. The inherent redundancy in fitting the complete 2D pattern compensates for this. (Inset) ^{15}N **A** tensor used in simulation.

As there are no hydrazide $^{14,15}N$ features to higher frequency, this $^{14,15}N$ must be the more strongly coupled of the two. It is invariably the case that a nitrogen bound to the Fe(III) of such a mixed-valence diiron center has a larger coupling than a similar one bound to the Fe(II).[55,57] This is largely a consequence of the spin coupling within the diiron center. If we write [$\mathbf{a^{III}}$, $\mathbf{a^{II}}$] as the intrinsic hyperfine tensors for nitrogen ligands of [Fe(III), Fe(II)] in the absence of the exchange coupling between Fe ions, then the hyperfine tensors observed for these ligands in the $S = {}^1/_2$ ground state of the coupled center are well known to take the form,[48]Thus, if the $\mathbf{a^{i,int}}$ for ligands to the two Fe

$$\mathbf{A^{III}} = K^{III}\mathbf{a^{III}} = (+\,7/3)\mathbf{a^{III,int}}\ \mathbf{A^{II}} = K^{II}\mathbf{a^{II}} = (-\,4/3)\mathbf{a^{II,int}} \quad (1)$$

ions are comparable, the observed couplings should be approximately twice as large for a ligand to Fe(III). Given the

(57) Gurbiel, R. J.; Doan, P. E.; Gassner, G. T.; Macke, T. J.; Case, D. A.; Ohnishi, T.; Fee, J. A.; Ballou, D. P.; Hoffman, B. M. *Biochemistry* **1996**, *35*, 7834−7845.

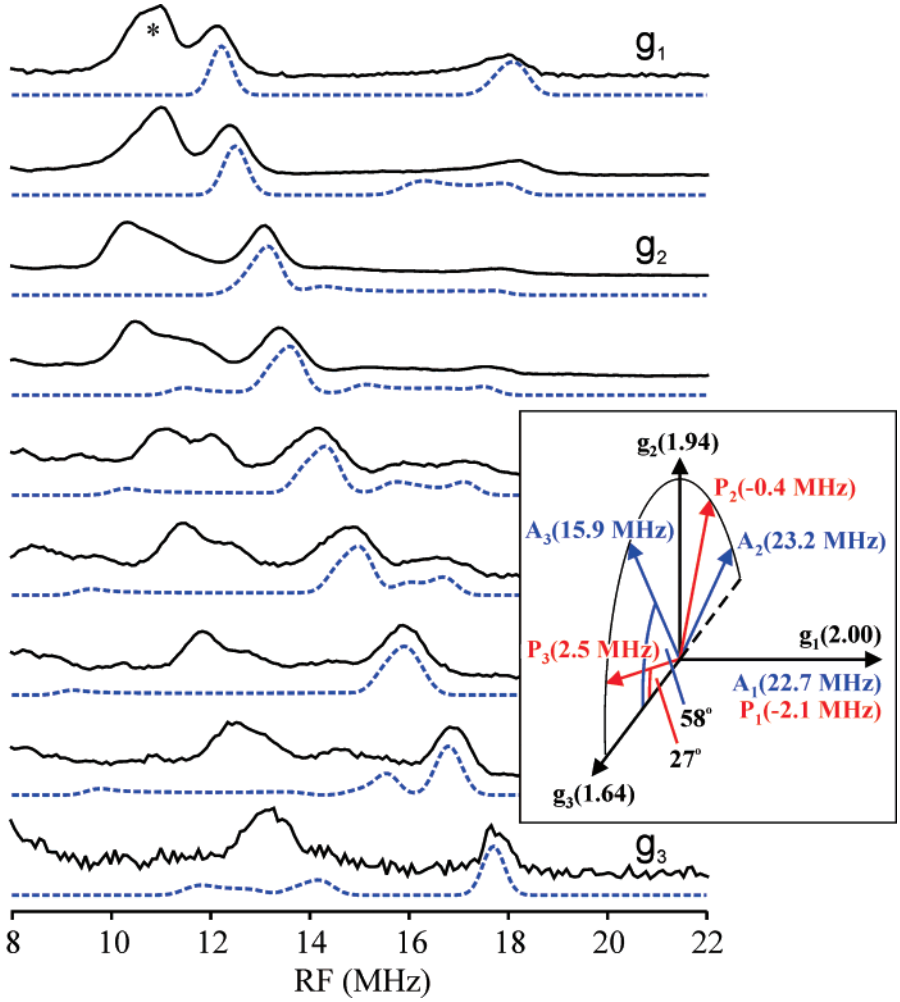

Figure 10. Simulated (blue) and experimental (black) 2D field-frequency plot of ^{14}N Davies ENDOR spectra for **1**, normalized to unity. The (*) at g_1 is a feature, seen in all spectra between 10 and 14 MHz, from ^{14}N of the β-diketiminate ligands and therefore are not included in the simulations. Conditions: π pulse length = 80 ns, τ = 700 ns, repetition time = 5 ms, MW frequency = 35.069 GHz. (Inset) ^{14}N **A** and **P** tensors used in simulation.

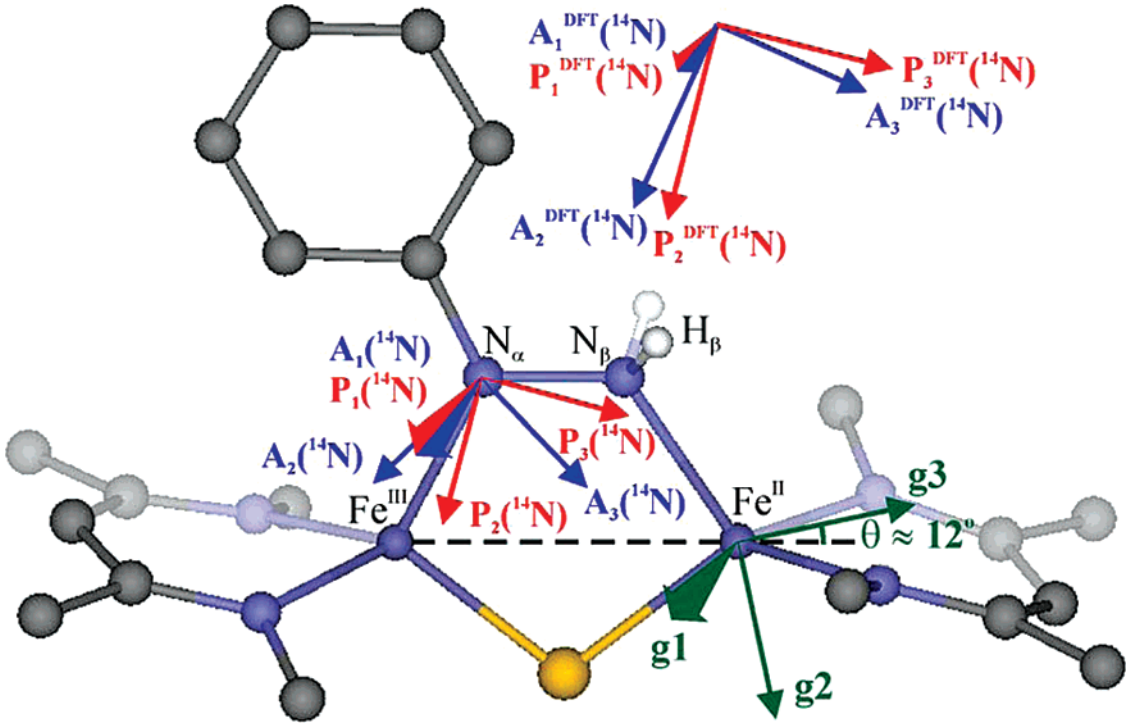

Figure 11. Experimentally determined **g** tensor, and ^{14}N **A** and **P** tensors from both simulation and DFT calculation, shown in molecular frame.

above assignment that the ferric ion is bound to the "internal" nitrogen Nα, the strongly coupled exchangeable ^{14,15}N signal is assigned as Nα.

Comparison of spectra taken at g_1 for **1**(^{15}N) and **1**(^{14}N) further reveals a $\nu_+ \approx 9$ MHz feature from the second nitrogen, ^{15}Nβ (Figure 8). According to eq S1 (see Supporting Information), this frequency corresponds to a ^{15}N hyperfine coupling of $|A(^{15}N\beta)| \approx 8$ MHz, about 1/4 that for Nα. This peak is visible with small variation in frequency for all fields from g_1 to g_3; any additional features that might arise as a consequence of an anisotropic hyperfine component are obscured by the signals from the nitrogen atoms of the β-diketiminate ligands. As a result, we may say that the anisotropic interaction for Nβ is likely to be small, and that $|a_{iso}(^{15}N\beta)| \approx 8$ MHz; unfortunately, a precise analysis of the Nβ hyperfine interaction was not possible.

The 2D ^{15}Nα ($I = {}^1/_2$) ENDOR pattern is well resolved from all other nitrogen signals at all fields and was readily simulated, Figure 9, yielding a hyperfine tensor that is essentially axial, $\mathbf{A}(^{15}N\alpha) = [-31.0(5), -32.5(5), -22.0(5)]$ ($A_\perp(^{15}N\alpha) \approx -32$ MHz, $A_{||}(^{15}N\alpha) = A_3 \approx -22$ MHz) MHz, with isotropic component, $a_{iso}(^{15}N\alpha) = -28.5(5)$ MHz, and anisotropic contribution, $\mathbf{T}(^{15}N\alpha) = [-2.5(7), -4.0(7), +6.5(7)]$ MHz. Although the fits show only that $A_\perp$ and $A_{||}$ have the same sign, we have assigned a negative sign for $a_{iso}(^{15}N\alpha)$, because the isotropic coupling for a ligand bound to a high-spin iron ion originates in the σ delocalization of spin into the sp^n donor orbital of the N ligand. The positive sign for the ^{15}Nα dipolar parameter, $2T(^{15}N\alpha) = +6.5$ MHz (negative sign for $2T(^{14}N\alpha)$) then is unexpected, as normally this contribution also originates from σ delocalization into the sp^n hybrid. We then take into account the additional negative sign of eq 1 and assign, $a_{iso}(^{15}N\beta) \sim +8$ MHz. The hyperfine parameters for ^{14}Nα/β are obtained from those of ^{15}Nα by multiplication with the appropriate ratio of nuclear g values, $g_n(^{14}N)/g_n(^{15}N) = -0.71$: $\mathbf{A}(^{14}N\alpha) \approx [22,23,16]$ MHz; $a_{iso}(^{14}N\beta) \approx -6$ MHz.

This best fit has A_3 normal to g_1 and in the $[g_2, g_3]$ plane, but not along either principal direction; the hyperfine tensor is rotated about g_1 relative to the corresponding **g** tensor axes by an angle ϕ(A) of 58° (the angle between g_3 and A_3) (Figure 9). As the nitrogens of the hydrazide lie in the molecular mirror plane that passes through the five-membered ring FeNNFeS, their hyperfine tensors, like **g**, must exhibit this mirror symmetry, which means that the unique ("parallel") component, A_3, can either lie along the principal g-value normal to the mirror plane or lie in the plane at an orientation not determined by symmetry. Thus, the placement of A_3 in the $[g_2, g_3]$ plane, but not along either g-value direction, shows that g_1 is normal to the symmetry plane, that contains $[g_2, g_3]$, a conclusion used above in the analysis of the ^{2}H ENDOR measurements.

The ^{14}Nα ($I = 1$) spectra of **1** exhibit a large quadrupole splitting, as indicated in the g_1 spectrum of **1** in Figure 8 and seen in the 2D field-frequency pattern for ^{14}Nα, Figure 10. The quadrupole interaction tensor for ^{14}Nα, $\mathbf{P}(^{14}N\alpha)$ also was determined with the aid of the molecular symmetry, as follows. As with $\mathbf{A}(^{14}N\alpha)$, the fact that ^{14}Nα lies in the molecular mirror plane requires that one principal axis of $\mathbf{P}(^{14}N\alpha)$ lies normal to the mirror plane, parallel to g_1. The magnitude of $P_1(^{14}N\alpha)$, the principal value along g_1, can be obtained by inspection, from the quadrupole splitting at g_1: $3P_1(^{14}N\alpha) = 6.3$ MHz. As **P** is traceless, $P_2 + P_3 = -P_1$, and only one more principal value must be determined. In addition we must determine the rotation of $\mathbf{P}(^{14}N\alpha)$ around g_1, which can be specified by the angle, ϕ-(P), between $P_3(^{14}N\alpha)$ and g_3. These two parameters were determined by performing simulations with a range of angles $0 \le \phi(P) < 180°$, in each case adjusting $P_2(^{14}N\alpha)$ and $P_3(^{14}N\alpha)$ so that the quadrupole splitting at g_3 matched the experimental spectrum. The quadrupole splittings in the 2D field-frequency pattern of Figure 10 are reproduced by a quadrupole tensor, $\mathbf{P}(^{14}N\alpha) = [-2.1(1), -0.4(1), 2.5(1)]$ MHz, where $P_1(^{14}N\alpha)$ lies along g_1, and $P_3(^{14}N\alpha)$ makes an angle of $\phi(P) = 27 \pm 2$ degrees with g_3. The sign of $\mathbf{P}(^{14}N\alpha)$ was chosen to agree with the DFT calculations as described below. The refined value of $\mathbf{A}(^{14}N\alpha)$ used in the simulation was [22.7(5), 23.2(5), 15.9(5)] MHz (Table 2).

Table 2. Calculated and Experimental **A** and **P** Tensors (MHz) of ^{14}Nα and ^{14}Nβ

		DFT			experiment		
^{14}Nα	**A**	17.5	24.2	29.0	22.7	23.2	15.7
	P	−2.2	−0.4	2.7	−2.1	−0.4	2.5
^{14}Nβ	**A**	−11.0	−6.5	−4.7	$a_{iso} \approx -6$		
	P	−1.4	−0.7	2.1			

One further ambiguity in tensor orientations was resolved by reference to the DFT computations. The ^{14}N ENDOR simulations reveal that the orientation of $\mathbf{A}(^{14}N\alpha)$ is related to that of **g** by a rotation of $\phi(A) = \pm 58°$ about g_1, whereas **P** is rotated $\phi(P) = \pm 27°$ about g_1. Both ϕ angles must have the same sign, but that sign is not determined by experiment, and thus there are two possible orientations for the **A** and **P** tensors in the molecular frame. The correct sign was taken to be that which leads to agreement between the orientations of $\mathbf{A/P}(^{14}N\alpha)$ and DFT-calculated interaction tensors, $\mathbf{P}^{DFT}(^{14}N\alpha)$. The quadrupole tensor is calculated from the charge density, not spin density, and the resulting expectation that a DFT calculation should give reliable results is borne out by the close agreement between the calculated, nearly rhombic quadrupole tensor components, $\mathbf{P}^{DFT}(^{14}N\alpha) = [-2.2, -0.4, 2.7]$ MHz, and the experimental components, $\mathbf{P}(^{14}N\alpha) = [-2.1, -0.4, 2.5]$ MHz (Table 2). This comparison shows that the values, $\phi(P) = -27°$, $\phi(A) = -58°$ are clearly correct, for with this choice of sign the experimental $\mathbf{P}(^{14}N\alpha)$ is coaxial with $\mathbf{P}^{DFT}(^{14}N\alpha)$ to within 1°; this quadrupole tensor is superimposed on the crystal structure of **1** in Figure 11.

Discussion

We have combined ^{1,2}H and ^{14,15}N ENDOR data, symmetry arguments, and point-dipole and DFT computations in an accurate, self-consistent determination of **g**, $\mathbf{A}(^2H\beta)$, $\mathbf{A}(N\alpha)$, and $\mathbf{P}(^{14}N\alpha)$, along with an approximate determination of $\mathbf{A}(N\beta)$ for the hydrazide that bridges the mixed-valence diiron center of **1**. The agreement between measured and calculated $\mathbf{T}(^2H\beta)$ confirm the simple expectation that the terminal Nβ binds to Fe(II) and that the central Nα binds to Fe(III). The existence of the molecular plane of symmetry of **1** that contains the FeNNFeS ring and bisects the Hβ−Nβ−Hβ angle requires that the **g** tensor and the **A**, **P** tensors of nuclei lying on the mirror plane each has a principal value directed normal to the plane. In addition, the two Hβ must be both chemically and magnetically equivalent and thus describable by identical tensors. All of the ENDOR data (^{1,2}H,^{14,15}N) were well analyzed through application of these constraints.

ENDOR experiments determine the principal values of the nuclear interaction tensors and their orientation within the **g** frame. The principal values of the dipolar ^{2}H interaction tensor, **T**(^{2}H), found by experiment are in good agreement with those predicted both by a simple point-dipole interaction with the spin-coupled diiron center $\mathbf{T}^{\mathbf{dip}}$(^{2}H)[54,55] and a broken-symmetry DFT calculation $\mathbf{T}^{\mathbf{DFT}}$(^{2}H). This agreement allowed us to determine the orientation of **g** and **A**(Hβ) in the molecular mirror plane *without* the ambiguities that typically inhere in such measurements. Likewise, the principal values of the computed ^{14}N quadrupole tensor, $\mathbf{P}^{\mathbf{DFT}}$(^{14}N$\alpha$), are in excellent agreement with those of the experimentally determined **P**(^{14}Nα), and this allows us to determine the orientations of **A**(Nα), **P**(^{14}Nα) in the molecular frame without ambiguity, Figures 7 and 11. The following discussion both addresses the issues raised and resolved by these measurements *and* indicates the ways in which our findings can be used to help characterize catalytic nitrogenase intermediates.

^{1,2}Hβ Hyperfine Interactions. The calculated principal values of $\mathbf{T}^{\mathbf{Dip/DFT}}$(^{2}H) are in good agreement with the experimentally determined **T**(^{2}H), as expected from our earlier studies of diiron centers. In the present case, we could calculate $\mathbf{T}^{\mathbf{Dip}}$ because we knew the (antiferromagnetic) nature of the spin-coupling within the diiron center to which the hydrazide is bound and the values for the spin-coupling coefficients, K^{III} and K^{II} relating intrinsic and observed couplings, as in eq 1. When studying intermediates trapped during the reduction of N_2 by nitrogenase we do *not* know the nature of the spin coupling. However, the confirmation here that point-dipole computations give accurate predictions of **T**(H) for an Fe-bound [$-NH_x$] means that we will be able to invert the process and to use experimentally determined **T**(^{1,2}H) to infer details of the spin coupling for the metal ions of an intermediate where FeMo-co binds a substrate-derived [$-NH_x$].

The experimental orientation of **A**(^{2}H) was determined by first orienting **A**(^{2}H) relative to **g** through ENDOR simulations, then adjusting the orientation of **g** ($\theta \approx 12°$) so that **A**(^{2}H) is most closely aligned with $\mathbf{T}^{\mathbf{Dip}}$(^{2}H). However, the high precision of these measurements discloses that **A**(^{2}H) and $\mathbf{T}^{\mathbf{Dip}}$(^{2}H) nevertheless are not exactly coaxial (Table 1). Comparison of the direction cosines and spherical polar angles (θ, ϕ) given in Table 1 reveals that **A**(^{2}H), which should lie in the FeFeH plane, is rotated about the molecular frame *z* axis (Fe$-$Fe vector) away from the FeNNFeS symmetry plane by about 7° more than is $\mathbf{T}^{\mathbf{dip/DFT}}$. This would occur if the N$\beta-$Hβ bond distance and/or H$\beta-$N$\beta-$Hβ bond angle were greater than that given by the crystal structure. X-ray crystal structure determinations systematically underestimate X$-$H distances by about 0.1 Å,[58] and the statistical random error is estimated to be about 0.07 Å in all directions; this can account for about half (~3°) of this difference. To account for the remaining difference would require a further translation of the proton position by 0.18 Å, corresponding to a bond distance increase from 1.02 to 1.12 Å, and a H$\beta-$N$\beta-$Hβ bond angle increase from 88 to 104°. Whether this small discrepancy is within the accuracies of the crystal and ENDOR structure determinations is not certain.

^{14,15}Nα,β Interactions. ^{14}N Quadrupole Coupling. The ^{14}N quadrupole interaction tensor, **P**, is characterized by the magnitude of its components (Table 2), its orientation, and its symmetry; the latter can be summarized in terms of the rhombicity parameter, $0 \le \eta \equiv |(P_2 - P_1)/P_3| \le 1$ ($P_3 = P_{max}$), which approaches zero in axial symmetry and has a maximum value, $\eta = 1$.

P can be qualitatively understood by applying the Townes-Dailey (TD) model for quadrupole couplings.[59] In this treatment, the principal values of **P** are scaled to the intrinsic coupling constant for a single electron in a nitrogen 2*p* orbital, $-|e^2qQ_0| \approx -(8-10)$ MHz;[60] and are proportional to π_i, the imbalance between the occupancies of the $2p_i$ orbital, $0 \le N_i \le 2$, $i = 1-3$:

$$P_i = -|e^2qQ_0|\pi_i\,\pi_i \equiv N_i - (N_j + N_k)/2$$

$$\eta = [\pi_2 - \pi_1]/\pi_3 = (3/2)\,[N_2 - N_1]/[N_3 - (N_1 + N_2)/2]$$

The quadrupole tensor thus is predicted to be rhombic when $\delta N_{12} = [N_1 - N_2] \approx \delta N_{23} = [N_2 - N_3]$.

To estimate **P** for the hydrazide "trigonal-planar" Nα, we label the out-of-plane $2p\pi$ orbital, $i = 1$; the other two 2p orbitals are combined with 2s to form three sp^2 hybrid σ orbitals, h_j, j = a$-$c, with occupancies n_j; we take hybrid h_a to point toward Fe, h_b toward C, and h_c toward N. For Nα of a "free" hydrazide anion in this geometry, the orbital occupancies would be $N_1 = 2$, $n_a = 2 > n_b > n_c$, where the Nα $2p\pi$ orbital occupancies arising from h_b and h_c are less than the total occupancy of the σ-bonds (2) because of covalent sharing with C and N, respectively. The net result of the orbital hybridization is, $N_1 > N_2 > N_3$, which corresponds to an ordering of the quadrupole principal values, $P_1 > P_2 > P_3$. Further taking $n_b \sim 1.3$, $n_c \approx 1$ for the occupancy of the sp^2 hybrids of free hydrazide, as suggested by analysis of nuclear quadrupole resonance data from reference molecules,[60] one gets $N_1 = 2 > N_2 \approx 1.7 > N_3 \approx 1.2$, yielding a highly rhombic tensor, $\eta \approx 0.7$. Bonding the hydrazide N to Fe(III) would further increase the rhombicity, for it would involve modest σ donation to Fe from h_a, reducing n_a, and thus N_2, but leaving N_1 and N_3 unchanged. Thus, the TD model accounts surprisingly well for the experimentally observed rhombicity of the trigonal Nα: $\eta(^{14}\text{N}\alpha) = 0.75$, and suggests that the experimental observation of a such a tensor is primarily a consequence of the bonding geometry.

The analysis further indicates that P_2 should point roughly along the Fe$-$N bond, although unequal covalencies of the N$-$C and N$-$N bonds, with $n_b > n_c$, will rotate the quadrupole tensor somewhat, so P_2 is not expected to point exactly along Fe$-$N. Thus, the TD approach provides a means of understanding the rhombicity and, roughly, the orientation of the quadrupole tensor. The heuristic nature of the TD approach, however, means that efforts to refine the TD tensor values and orientation are unwarranted.

DFT computations go far beyond the heuristic description of TD, and we find that $\mathbf{P}^{\mathbf{DFT}}$(^{14}N$\alpha$) matches both the principal values (Table 2) and orientation (Figure 11) of **P**(^{14}Nα) for the hydrazido nitrogen (Nα) very well; in fact, this agreement allowed us to resolve the last ambiguities in assigning the orientations of the experimental **P** and **A** tensors. Such agreement between theory and experiment for **P** is not unexpected

(58) Stout, G. H.; Jensen, L. H. *X-ray Structure Determination: A Practical Guide*, 2nd ed.; Wiley: New York, 1989.

(59) Townes, C. H.; Dailey, B. P. *J. Chem. Phys.* **1949**, *17*, 782−796.

(60) Lucken, E. A. C. *Nuclear Quadrupole Coupling Constants*; Academic Press: New York, 1969.

because $\mathbf{P}(^{14}N)$ for a N bound to a metal ion of a spin-coupled center, such as **1** *or* FeMo-co, is determined by the local environment of the N, is dependent on *charge* not *spin* density in the vicinity, and is *not* sensitive to spin coupling within the center. This confirmation of the accuracy of $\mathbf{P}^{\mathbf{DFT}}(^{14}N\alpha)$ for the metal-bound hydrazido nitrogen of a well-defined biomimetic model suggests that $\mathbf{P}^{\mathbf{DFT}}(^{14}N\beta)$ for the terminal "hydrazino" nitrogen *and for other nitrogenous* species will be comparably accurate. Beyond that, the quadrupole interaction of a nitrogen bound to a spin-coupled multimetallic center is independent of the details of spin coupling and the spin-coupling coefficients. Hence, the present study supports the joint use of $\mathbf{P}(^{14}N)$ transferred from model compounds and calculated $\mathbf{P}^{\mathbf{DFT}}$ in testing a proposed structure for the N_2-derived fragment bound to FeMo-co of a nitrogenase intermediate.

Indeed, we may go further and propose that the quadrupole interactions will provide excellent signatures of such structures. Comparison of the principal values of **P** for the trigonal and four-coordinate ^{14}N shows that the largest tensor components are roughly comparable, but that the tensor of the trigonal Nα is much more rhombic: $\eta(^{14}N\alpha) = 0.75$, $\eta^{\mathbf{DFT}}(^{14}N\alpha) = 0.67$, compared to $\eta^{\mathbf{DFT}}(^{14}N\beta) = 0.33$ calculated from $\mathbf{P}^{\mathbf{DFT}}(^{14}N\beta)$. On the other hand, an end-on bound nitrogen N_2 or a bound NH_3 have axial/3-fold symmetry, respectively, and both must have quadrupole tensors with axial symmetry, $\eta \rightarrow 0$. Thus, the present results suggest that the ^{14}N quadrupole tensor(s) of a nitrogenous moiety bound to FeMo-co of a nitrogenase intermediate will provide a powerful tool in identifying the moiety (e.g., Chart 1).

^{14,15}N Hyperfine Coupling. The isotropic coupling dominates the hyperfine interactions of metal-bound $^{14,15}N$, and this parameter thus provides the best reference for comparison to experimentally determined quantities for FeMo-co. The intrinsic isotropic coupling for the amido $^{15}N\alpha$ bound to Fe(III) is $a_{iso}^{III,int}(^{15}N\alpha) = (3/7)\cdot(-28.5) \approx -12$ MHz; that for the amino $^{15}N\beta$ bound to Fe(II) is half as big, $a_{iso}^{II,int}(^{15}N\beta) \approx -(3/4)\cdot(+8) \approx -6$ MHz. The intrinsic coupling for the N bound to the spherically symmetric Fe(III) is likely to be transferrable to other centers. That for N bound to Fe(II) may be less precisely transferrable, as bonding to Fe(II) is "directional".

The isotropic hyperfine couplings calculated by DFT are in approximate agreement with those measured, whereas the anisotropic contributions to $\mathbf{A}(^{14}N\alpha)$ and $\mathbf{A}^{\mathbf{DFT}}(^{14}N\alpha)$ are not in particularly good agreement (Table 2). This limited agreement is not surprising, for calculation of **A** is inherently more difficult than that of **P** because the spin density is a difference between up and down spin densities and, hence, intrinsically less reliable than the charge density, their sum, which is used to calculate **P**. This difficulty is compounded by the fact that the calculation of **A** for a spin-coupled center employs the BS algorithm, which introduces additional approximations.[48] Finally, because $\mathbf{A}(^{14}N\alpha)$ is largely isotropic, as expected for a nitrogen directly bound to the Fe(III), both the orientation of $\mathbf{A}(^{14}N\alpha)$, which is derived from the smaller anisotropic component, and the anisotropic components themselves are hard to predict. Indeed, the calculations predict a rhombic anisotropic interaction, whereas the experimental one is roughly axial, as is normally the case because the anisotropic hyperfine interaction arises from spin density in the p-orbital that contributes to the sp^n donor orbital of N. In addition, the orientation of $\mathbf{A}^{\mathbf{DFT}}(^{14}N\alpha)$ is not in good agreement with that of **A**, being rotated by 24°.

The hyperfine coupling for a nitrogenous species bound to the FeMo-co of nitrogenase would be given by an equation analogous to eq 2, but as noted above, the K "scale factor" would be unknown. However, the values of a_{iso} measured here for N can be used to discuss both the spin state of an Fe that binds a substrate-derived fragment and the spin-coupling scheme of FeMo-co in the intermediate. As an example, the nitrogenase intermediate formed during the reduction of hydrazine contains an $[-NH_x]$ fragment for which $a_{iso}(^{15}N) \approx 1.9$ MHz, which is much smaller than the values measured in **1** (12 MHz to anionic N; 6 MHz to neutral N).[61] If this fragment were bound *either* to a high-spin Fe(II) or Fe(III), the intrinsic couplings measured here indicate that the ion would have to have a very small spin-coupling coefficient, $K \lesssim 0.2-0.3$. However, these $a_{iso}(^{15}N)$ are so low that it suggests as a real possibility that the coordinating Fe ion is intermediate or even low spin, not high spin. When a nitrogen is bound to an intermediate-spin Fe ion, the intrinsic hyperfine coupling generally arises from spin polarization of an Fe−N/d-σ bond by spin in an Fe d-π orbital, rather than direct delocalization through overlap with a spin-bearing d-σ orbital, and hence would be much lower than measured here for **1**.

In summary, we have used a novel strategy for combining ENDOR analysis procedures, symmetry constraints, and computational techniques to determine for the first time the interaction parameters for a well-defined, biomimetic complex for nitrogenase, **1**. We report the intrinsic hyperfine tensors for nitrogen atoms of the bound hydrazine in **1**, the quadrupole tensor for the hydrazido $^{14}N\alpha$, and the hyperfine tensor for the Hβ, obtaining not only the tensor principal values but also unambiguous tensor orientations relative to the molecular frame. The interaction tensor principal values can be used to test the identity of a product of N_2 reduction bound to FeMo-co.[62] This study further shows that the ^{14}N quadrupole and ^{1}H hyperfine tensors calculated by DFT methods accurately reproduce experiment, thereby validating the use of DFT computations in studying nitrogenous species bound to FeMo-co of a trapped nitrogenase intermediate.

Acknowledgment. This work has been supported by the NIH (HL 13531, BMH; GM065313 PLH). We thank Dr. Louis Noodleman for sharing a script to exchange spin densities of the ADF output file. We thank Dr. Javier Vela for preparation of initial ENDOR samples.

Supporting Information Available: Experimental details, Figure S1, and Appendix I. This material is available free of charge via the Internet at http://pubs.acs.org.

JA073934X

(61) This relies on the unvarying observation that the isotropic term dominates the hyperfine interaction for a N ligand to a metal ion.
(62) It is unlikely that tensor orientations relative to the FeMo-co plane can be determined.